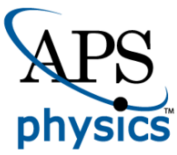

Internal gravity waves generated by an impulsive plume

Alan Brandt and Kara R. Shipley

Phys. Rev. Fluids **4**, 014803 — Published 14 January 2019

DOI: 10.1103/PhysRevFluids.4.014803

Internal gravity waves generated by an impulsive plume

Alan Brandt, Kara R. Shipley
Johns Hopkins University Applied Physics Laboratory, Laurel MD 20723, USA

A series of laboratory experiments on the generation of internal waves by a short duration impulsive, turbulent, forced plume descending into a stratified layer has been conducted. After the plume descends to a maximum depth it rebounds to an equilibrium level where the ensuing oscillation results in the generation of a propagating internal wavefield. The finite duration impulsive plumes exhibited two classes of behavior: (1) plumes with a density that matched that of the bottom of the stratified layer had a constant fraction of the plume energy transferred to the internal wavefield, with an average value of $E_{IW}/E_P \cong 6\%$, independent of the duration of the plume release. In contrast, (2) plumes with lower densities, half that of the bottom of the stratified layer, exhibited a larger degree of coupling of the plume energy to the internal wavefield that increased with the duration of the plume release, having an average value of $\cong$ 10%. The observed degree of internal wave energy coupling for impulsive plumes is in general agreement with prior studies of continuous convective plumes and descending buoyant parcels.

I. INTRODUCTION

Outflows of plumes and jets into stratified environments result from natural and anthropomorphic sources including volcanoes, hydrothermal vents gaseous eruptions, room ventilation, sewage outflows, etc., as discussed by Turner [1] and Woods [2]. In the atmosphere and ocean short duration impulsive or intermittent plumes as opposed to continuous emissions often occur, for example due to storm events, and time dependent sewage outflows. In situations where the background environment is stratified both plumes and jets will generate internal waves that propagate away from the source. This study is focused on the generation of internal waves by intermittent turbulent forced plumes, and on the estimation of the fraction of energy in the plume that is transferred to the internal wavefield.

There is a long history of turbulent plume/jet/fountain studies focused on steady outflows, c.f. reviews by List [3], Kaye [4], Hunt and Burridge [5] as well as [1, 2]. However, few consider the internal wavefield generated when the plumes evolve in stratified environments. Even more limited are studies of intermittent plumes in stratified environments. In contrast to continuous plumes, the physical processes associated with intermittent events are inherently unsteady, transient and broad-band in nature.

Virtually all contemporary studies of turbulent buoyant plume evolution stem from the seminal paper by Morton, Taylor and Turner [6] and the extension of this approach to forced plumes (i.e. initial forcing due to buoyancy and momentum) by Morton [7]. The initial analysis and experiments [6] considered both continuous and instantaneous (finite volume) plumes in both uniform density and linearly stratified backgrounds. The results of [7] have been validated

for continuous plumes [8]; however [7] did not consider either instantaneous plumes as considered in the present study, or the nature of the internal wavefield.

Most studies of turbulent plumes in stratified environments have focused on continuous releases and measurements, usually on a sharp pycnocline interface. These studies generally focus on the penetration, entrainment, and the resulting intrusions, while a few have noted the generation of internal waves. In an analytic study of internal waves (IW) generated on an atmospheric inversion layer due to penetrative convection, Stull [9] found that the energy level of the IW excited varied considerably based on the strength of the inversion and the local lapse rate up to a maximum of 68% of the energy of the convective disturbances. Particularly noteworthy is the laboratory investigation by Ansong and Sutherland [8], where buoyant plumes entering a linearly stratified layer were found to lose from 0.1% to 8% (~4% on average) of the plume energy to the internal wavefield, i.e. the ratio of internal wave energy to the initial plume energy, E_{IW}/E_P ~4%. The IW field energy was concentrated at the neutral buoyancy level, i.e. where the mixed plume/ambient fluid settled, and the IW forcing occurred mainly due to the plume rebound, the latter of which was also noted in [10]. More recently Ezhova *et al.* [11] numerically investigated the IW field resulting from a turbulent jet impinging on a thermocline. It was determined that the ratio of the IW energy flux to the jet energy flux depended on the thermocline thickness. For thin thermoclines E_{IW}/E_{jet} was ~4% - 5%, while for thick thermocline layers the ratio was approximately half of that.

Only a limited number of fundamental studies of unsteady pulsed (intermittent) plume forcing of IW presently exist. In the context of atmospheric IW generation, the release of a buoyant plume was studied using a 2D numerical simulation by Clark *et al*. [12] and experimentally by McLaren *et al.* [10]. Clark *et al.* [12] considered the atmospheric internal waves generated by boundary layer shear combined with thermal forcing of moist air. While it was found that the shear was more efficient in forcing IW than pure thermal forcing, both mechanisms were transient in nature and resulted in coherent wave patterns, with moist (thermal) forcing producing noticeable correlations between the internal wavefield (cloud field) and the boundary layer eddies. These boundary layer forced IW are not unlike turbulent wake generated IW. In the experiments of McLaren *et al*. [10] a small volume of miscible fluid was released in a continuously stratified fluid and the IW motions were observed by tracking neutrally buoyant beads. It was observed that the induced IW field was inhomogeneous and transient in nature with a wide spectrum of wave periods, from one to four times the Brunt-Väisälä period, and was tied to the oscillation of the released fluid. Noh *et al.* [13] observed the generation of linear and nonlinear solitary waves on a thin density interface that resulted from the impingement of a buoyant thermal; spectral content and propagation speeds were measured. Experiments on IW generation by the release of a buoyant parcel into a linearly stratified environment were performed by Cerasoli [14]. In these experiments the released fluid mass had a density larger than the density of the bottom of the stratified layer. This released mass mixed with the ambient fluid and came to rest at a neutral depth where internal waves were generated. The internal wave energy was reported to be 20% - 25% of the change in the system potential energy resulting from the parcel release.

In the present study an impulsive forced plume was released into a finite thickness stratified layer so that measurements of the total IW energy could be obtained and compared to the energy of the forcing plume. Scaling relationships for the finite time plume release and the IW energy are presented in § II. The experimental configuration is described in § III and the results in § IV. Section V presents a summary and discussion.

II. SCALING RELATIONSHIPS

To investigate the extent of energy transfer from a descending plume in a stratified environment to the internal wavefield, a series of experiments were conducted where the duration of the impulsive plume release, ΔT, the density of the plume, ρ_p, and the thickness of the stratified layer, H, were varied. The orifice exit radius was fixed at b_0 = 0.64 cm and the density gradient in the stratified layer was fixed at a nominal value of $N \cong 1$ s^{-1}, where N is the buoyancy frequency defined (with vertical direction z defined as positive in the downward direction) as

$$N = \left(\frac{g}{\rho_0}\frac{d\rho}{dz}\right)^{1/2}, \tag{1}$$

where $\rho = \rho(z)$ is the density gradient as a function of depth, z, ρ_0 is a reference density of the ambient fluid at the orifice exit, that of fresh water, and g is the gravitational acceleration. As the exit velocity, w_0, was essentially constant for all cases at $w_0 \cong 6.5$ cm/s (discussed in § III) the Reynolds number for all cases was $Re = w_0 2b_0/\upsilon \cong 832$ and the internal Froude number was, $Fr = w_0/Nb_0 \cong 10.2$. For the present experiment, the ratio of the input slug length to its diameter can be defined as an initial plume Froude number

$$Fr_0 = w_0\,\Delta T/b_0. \tag{2}$$

As ΔT nominally varied from 0.5 s to 2.5 s, Fr_0 ranged from ≅ 5 to 25. (Since b_0 is constant for these experiments and w_0 varies very little, $Fr_0 \propto \Delta T$.)

A. Plume properties

The relationships defining the properties of buoyant and forced plumes were first outlined in [6, 7]; however for clarity the terminology of [8, 15] will be used and extended to the present case where the duration of the plume release is finite. The release of a turbulent plume of density ρ_p can be characterized in terms of its initial conditions, i.e. its properties at the point of release that are assumed to approximate top-hat profiles. The momentum flux, M_0, and the buoyancy flux, B_0, are

$$M_0 = \pi b_0^2 w_0^2\,, \tag{3}$$

$$B_0 = \pi b_0^2 w_0 g_0{}'\,, \tag{4}$$

where b_0 is the radius of the exit orifice and $g_0{}'$ the reduced gravity defined as

$$g_0{}' = g\,\frac{\rho_p - \rho_0}{\rho_0}\,. \tag{5}$$

Combining (3) and (4) results in the intrinsic length scale

$$L_0 = M_0^{3/4} B_0^{-1/2}\,, \tag{6}$$

which is a measure of the vertical distance over which the inertia of the system is dominates the buoyancy and is calculated directly from the momentum and buoyancy fluxes. That is, the intrinsic length scale, L_0, denotes the distance from the release point at which the forced plume transitions from acting as a jet to acting as a buoyant plume.

For a plume exiting into a linearly stratified fluid, the ratio of the effects of momentum and buoyancy (jet verses buoyant plume like behavior) is indicated by the flux ratio, σ, defined as

$$\sigma = \left(\frac{NM_0}{B_0}\right)^2 = \left(\frac{Nw_0}{g_0{}'}\right)^2. \tag{7}$$

The total energy of the plume as it exits the orifice is the sum of its kinetic energy and potential energy. The initial kinetic energy is

$$E_{P,ke} = \tfrac{1}{2} m w_0^2 = \tfrac{1}{2}\pi b_0^2 \rho_p w_0^3 \Delta T, \tag{8}$$

where m is the plume mass calculated from the volume injected during the finite impulse of duration ΔT at velocity w_0.

The initial potential energy of the plume is given by the displacement of ambient fluid by the buoyant force of the plume volume of fluid injected as

$$E_{P,pe} = \pi b_0^2\, g_0{}'\rho_p \int_0^{z_{final}} z\, dz = \tfrac{1}{2}\pi b_0^2\, g_0{}'\rho_p z^2|^{z=w_0\Delta T} = \tfrac{1}{2}\pi b_0^2 \rho_p g_0{}' w_0^2 \Delta T^2. \tag{9}$$

The resulting total plume energy is therefore

$$E_P = E_{P,ke} + E_{P,pe} = \tfrac{1}{2}\pi b_0^2 \rho_p w_0^2 \Delta T (w_0 + g_0{}'\Delta T)\,. \tag{10}$$

B. Internal wavefield properties

In the present study the internal wavefield is measured using a vertical array of conductivity probes spanning the stratified layer of thickness H, at a fixed radial distance from the plume center, R. The internal wave potential energy at any given time is the integral of the isopycnal displacements, η as

$$E_{IW,pe} = \int_0^H \tfrac{1}{2}\rho(z)\,\eta^2\,N^2\,dz\,. \tag{11}$$

The total potential energy of the internal wavefield generated by the plume is the integral of $E_{IW,pe}$ over the length of the wave packet, which corresponds to the wave phase speed, c_w, and the time interval during which the wave packet passes over the stationary probe rake, Δt. Assuming the IW field is radially symmetric (discussed further below), and that there is

equipartition between the internal wave potential and kinetic energy, the total internal wave energy, $E_{IW,}$ is

$$E_{IW} = 2\,(2\pi R)\,c_w \int_0^{\Delta t} E_{IW,pe}\,dt = 2\pi\,R\,c_w \int_0^{\Delta t}\int_0^{H} \rho(z)\,\eta^2\,N^2\,dz\,dt\,. \qquad (12)$$

The integration over H is performed as a discretized summation of the individual probe displacements. It should be noted that in this calculation all of the terms are measured quantities, based on the experimental configuration and the internal wavefield measurements (notably c_w, Δt, and η).

III. EXPERIMENTAL CONFIGURATION

The experiments presented herein examine the dynamics of a downward release of an impulsive plume of homogeneous heavy fluid into a fluid with a density-stratified layer above a region of constant density in a tank with dimensions 0.61 m wide x 1.22 m long x 1.83 m deep, shown schematically in Fig. 1. The plume exit orifice radius is b_0 = 0.64 cm and was located at the center of the tank width, i.e. 0.305 m from the tank walls. The probe rake tips (i.e. the sensing elements) were positioned laterally 0.66 m from the center of the exit valve. These distances are sufficiently large compared to the plume width (discussed in § IV.A) so that the plume evolution would not be affected by the presence of the tank walls. As the maximum plume width was generally less than 10 cm during the time interval that the internal waves were generated the rake was O(60 cm) from the plume edge, so that the probe rake measurements are that of the IW field and not those of the plume eddies.

The plume was visualized using fluorescent dye that allows for measurements of the plume dimensions as it evolves and thus computation of the plume energy flux. The internal wavefield in a representative radial plane was characterized by measuring the wave amplitudes using an array of conductivity probes. The use of particle imaging velocimetry (PIV) to measure the internal wavefield was considered but as it would necessitate refractive index matching and a distribution of seed particles that match the density at each level in the stratified layer it would have significantly complicated the experimental procedure. Use of a rake with closely spaced probes that directly measure internal wave amplitudes provides a reasonably continuous view of the IW field within a measurement plane that spans the entire stratified region with sufficient resolution to give an accurate measurement of the total internal wavefield energy. Such a conductivity rake has been successfully used to measure the internal wavefield and the wavefield energy in previously published studies (e.g. Brandt & Rottier [16]).

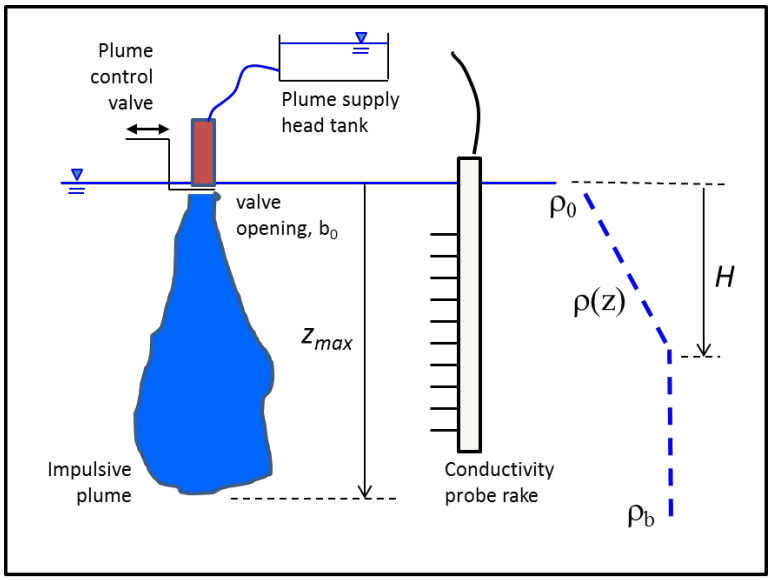

Figure 1. Schematic of experimental configuration.

A. Stratification

The tank was linearly stratified over a depth H using a computer controlled filling system that used fresh water and brine supply tanks. The fresh water density at the top was ρ_0, and the density at depths equal to and greater than H was constant, ρ_b, as shown in Fig. 1. To facilitate optimal use of the filling system and measurement of the plume exit velocity a thin 2 cm layer of fresh water was placed just below the plume exit valve. Two nominal values of H were used, 10 cm and 20 cm. In all cases, the surface was fresh water, $\rho_0 \cong 1$ g/cm^3. For $H \cong 10$ cm, the bottom salinity was $\rho_b \cong 1.011$ g/cm^3 (17 ppt salt), and for $H \cong 20$ cm, $\rho_b \cong 1.020$ g/cm^3 (31 ppt salt). The density gradient in the stratified layer was measured using a vertically traversing conductivity-temperature probe calibrated using premixed standard solutions. The buoyancy frequency was held constant at a nominal value of $N = 1$ s^{-1}, measured as the mean slope of the density gradient and calculated using (1). The tank stratification was measured prior to each run and changed when the density profile (primarily widening of the interfaces at the top and bottom of the stratified layer) deviated by more than 10%, generally after five runs.

B. Plume measurements

The plume was released using a control valve just below the surface of the water, with an exit orifice of radius b_0 = 0.64 cm. The plume control valve consisted of a motor actuated sliding plate that moved across the exit valve at high speed exposing a hole over the exit valve when opened and moved back to cover the valve after a prescribed time**.** The duration of the plume, i.e. the time the valve was open, ΔT, was varied nominally from 0.5 s to 2.5 s. The plume supply tank was kept at a constant pressure head utilizing a pump driven constant head tank system to ensure uniform, repeatable plume injection. The injected plume fluid had a

homogenous density, ρ_p, which is expressed in a non-dimensional form as a fraction of the top to bottom layer density, ρ_r

$$\rho_r = \frac{\rho_p - \rho_0}{\rho_b - \rho_0}. \tag{13}$$

Fluorescent dye (fluorescein) was added to the plume supply tank and was illuminated in the tank using an Nd-YAG laser sheet ~3 mm thick aligned along the centerline of the orifice, spanning the tank depth. Data were captured at a rate of 10 Hz using a Photron high-speed camera with a 75-300 Nikon zoom lens. Figure 2 shows a representative plume time series colored by the intensity of the dye fluorescence, which is proportional to the dye concentration.

The plume initial velocity, w_0, at the valve exit was measured using a PIV arrangement developed for this purpose. For these measurements, the plume was actuated in the same manner as during the experimental data runs, however, the dye was replaced with 13 µm silver coated hollow glass spheres, which are approximately neutrally buoyant in the upper 2 cm unstratified layer, and small enough to follow the local flow. PIV images were collected at 15 Hz with 8 ms between image pairs. These data were analyzed using DaVis PIV software and exported to MATLAB for analysis. Seven runs with nominally equal resolution were analyzed and aligned to a fixed uniform grid. At each time step, the velocity data were averaged over a 1 cm width below the center of the orifice, 0.37 cm below the orifice exit. This spacing was considered necessary to exclude any boundary effects from masking the orifice in the PIV data processing. As the release time of the impulsive plume ranged from 0.5 s - 2.5 s, the exit velocity data was fit to a functional form over 3.5 s to encompass the relevant time without over-constraining the fit. While w_0 varied as a function of the time from the valve opening, the resulting values of w_0 over the 0.5 s - 2.5 s interval were essentially constant at $w_0 = 6.5$ cm/s with standard deviation of only 3.1% of the mean over all experimental runs.

During the test runs, the exact time the valve was open was measured by recording the voltage pulse generated when a sensor attached to the spring loaded valve was open. However, there was not an automatic method to synchronize the start of the flow to the plume image frame number. Instead, the start of the run was determined empirically from observations of the plume. The error in the identification of the exact start of the plume with respect to the PIV images and the internal wavefield measurements during the test runs is estimated to be ± 0.1 s. The same empirical method of plume start selection was used for the plume evolution fluorescent dye data.

C. Internal wave measurements

The internal waves were measured with a stationary conductivity probe rake located at *R* = 66 cm from the orifice center, 28 cm from the back wall of the tank, and along the centerline of the tank width. The rake consisted of 17 conductivity probes spaced 1 cm apart, spanning the stratified region, *H*, providing a means to measure the total internal wave potential energy (only the probes within the stratified layer were used for analysis). For cases where additional

probes were needed to span the stratified region, the internal wave potential energy was scaled by the missing number of probes. The probe rake was calibrated prior to the test runs by vertically moving the rake over fixed distances spanning the anticipated range of isopycnal displacements, yielding a depth-conductivity calibration curve for each probe.

As the probes were stationary, vertical movements of the fluid due to the passage of the internal wavefield resulted in changes in conductivity that were converted to wave amplitudes as functions of time, $\eta(t)$. The resulting internal wave displacements were then averaged over the stratified layer and over the duration of the propagating plume generated wave packet to compute the internal wavefield potential energy in accordance with (11) and (12).

IV. RESULTS

The laboratory experiments were designed to measure the degree of energy transfer from an intermittent turbulent plume descending into a stratified layer. The descending plume entrains ambient fluid and subsequently rebounds to an equilibrium level, as illustrated in Fig. 2. As the plume descends into the stratified layer, and particularly on its rebound, internal waves are generated throughout the stratified layer. In addition when the plume penetrates the stratified layer into the uniform layer below and then rebounds internal waves can be generated at the interface. As the rake of conductivity probes spans the entire stratified layer the wave amplitudes measured consist of waves forced by all generating mechanisms.

As the plume is turbulent, the internal wavefield is not strongly coherent, analogous to turbulence generated waves from the wake of a body [17] and in contrast to the coherent waveforms generated due to the lee waves over a towed body [16]. Moreover, the turbulent plume is not instantaneously circumferentially coherent so the generated internal wavefield is not expected to be circumferentially coherent. However, as discussed below, the multiple runs in each test series conducted at fixed conditions over a range of ΔT are expected to be representative of the circumferentially averaged wavefield.

The effects of variations of the plume release time, ΔT, the plume density, ρ_p, and the stratified layer thickness, *H* on the generation of internal waves within the stratified layer were investigated. Two plume salinity settings were used, the first nominally matching the tank bottom salinity and the second nominally set to half the bottom salinity, resulting in values of $\rho_r \cong 1$ and ½. Stratified layer thicknesses of 10 cm and 20 cm were used. In all cases, the uniformly stratified region had a nominal buoyancy frequency of $N \cong 1$ s^{-1}. The average values of *H*, ρ_r, and *N* for each run series along with their standard deviations are shown in Table 1. Also shown is the number of runs in each series wherein ΔT was varied. (Series C has a larger number of runs than the other series because laboratory test conditions allowed for a higher percentage of runs with good quality data.)

Table 1. Run conditions by test series. Values ± 1 std. dev.

Series	# Runs	H (cm)	N (s^{-1})	ρ_r	E_{IW}/E_P
A	10	21.7 ± 0.2	0.97 ± 0.02	1.12 ± 0.07	0.062 ± 0.025
B	9	21.9 ± 0.3	0.96 ± 0.01	0.57 ± 0.01	0.110 ± 0.035
C	19	12.2 ± 0.7	0.91 ± 0.08	1.13 ± 0.17	0.066 ± 0.028
D	9	12.3 ± 0.6	0.93 ± 0.06	0.43 ± 0.05	0.092 ± 0.041

A. Impulsive plume

Figure 2 shows the time evolution of a representative plume cross-section at five instances directly under the orifice with the intensity of the dye fluorescence (above the background) artificially colored. The dye initially descends to a maximum depth, z_{max}, (panel 3) and then rebounds, expanding horizontally and concentrating at the neutral buoyancy depth, z_n (panel 5). Values of z_{max} and z_n for each run were obtained from the plume time series evolution described below, as illustrated in Fig. 3.

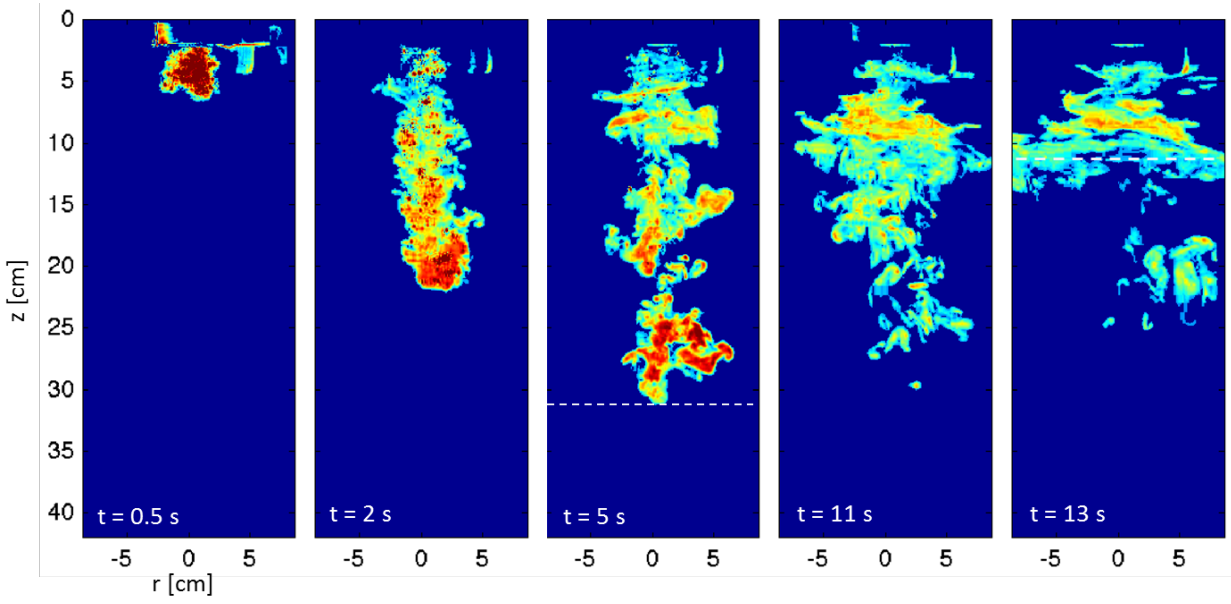

Figure 2. Turbulent plume time evolution as captured by the fluorescent dye and artificially colored based on intensity. Data shown is from Series C, Run 12, H = 11.9 cm, N = 0.95 s^{-1}, ρ_r = 1.17, ΔT = 1.73 s, z_{max} = 31.2 cm, and z_n = 11.1 cm. Successive images are ΔT = 0.5, 2, 5, 7, 11, 13 s. z_{max} and z_n are shown by the dashed lines in panels 3 and 5, respectively.

The temporal evolution of depth and width for two representative plumes is shown in Fig. 3. Fig. 3(a) is from Series C, (H = 14 cm, ρ_r = 1.49, ΔT = 1.68 s). At each time step and depth,

the dye is integrated along the width of a fixed cross-section of the tank, shown by the color bar. An integration window width of 17.2 cm which spans the plume width was used. The maximum depth for Run 19 is z_{max}= 35.3 cm occurring 5 s after the plume release. The dyed plume rebounds to z_n = 16.7 cm, indicated in the figure by the dark red band starting around 15 s. In this run, the plume descends and rebounds with limited oscillation about the neutral buoyancy depth. Residual dye can be observed outside of the neutral buoyancy depth. Run 66 from Series B (H = 21.7 cm, ρ_r = 0.58, ΔT = 1.83 s) is shown in Fig. 3(b). In contrast to the case of Fig. 3(a), the plume oscillates significantly about the neutral buoyancy depth, z_n = 17.9 cm, after rebounding and without much residual dye outside this band. In general, plume behavior for the thick stratified layer runs, $H \cong$ 20 cm, showed a higher degree of oscillation, as in Fig. 3(b), than the $H \cong$ 10 cm runs, as in Fig. 3(a). Since the plume is turbulent, time series of the dyed plume evolution using horizontal spatial averages, as shown in Fig. 3, were used to measure z_{max} and z_n.

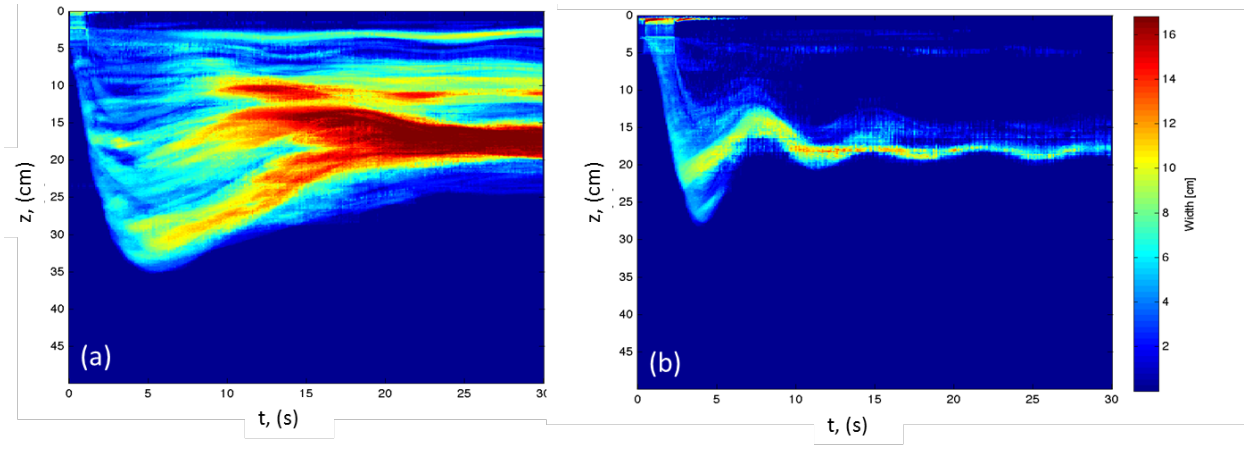

Figure 3. Plume width as a function of depth and time, evaluated over a cross-sectional window of 17.2 cm. (a) Series C, Run 19, H = 14.0 cm, ρ_r = 1.49, ΔT = 1.68 s, z_{max} = 35.3 cm, z_n = 16.7 cm. (b) Series B, Run 66, H = 21.7 cm, ρ_r = 0.58, ΔT = 1.83 s, z_{max} = 28.2 cm, z_n = 17.9 cm.

The plume release duration had a direct impact on the maximum depth of the plume for the smaller stratified layer thickness, $H \cong$ 10 cm, as would be expected, with a longer release correlating to a deeper plume, shown in Fig. 4. For Series C & D ($H \cong$ 10 cm), the plume penetration at larger values of $N\Delta T$ was significantly greater than the stratified layer depth. In contrast, for the $H \cong$ 20 cm runs, z_{max} was generally independent of $N\Delta T$ and only ~20% greater than H. This is the result of the larger contribution of the plume momentum as compared to its buoyancy; larger values of σ as shown in Fig. 5(b) cause greater jet like behavior and increased entrainment.

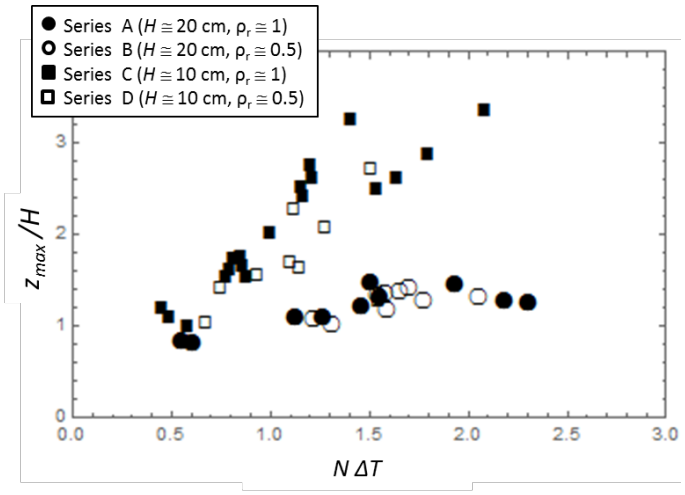

Figure 4. Plume maximum depth vs. release duration.

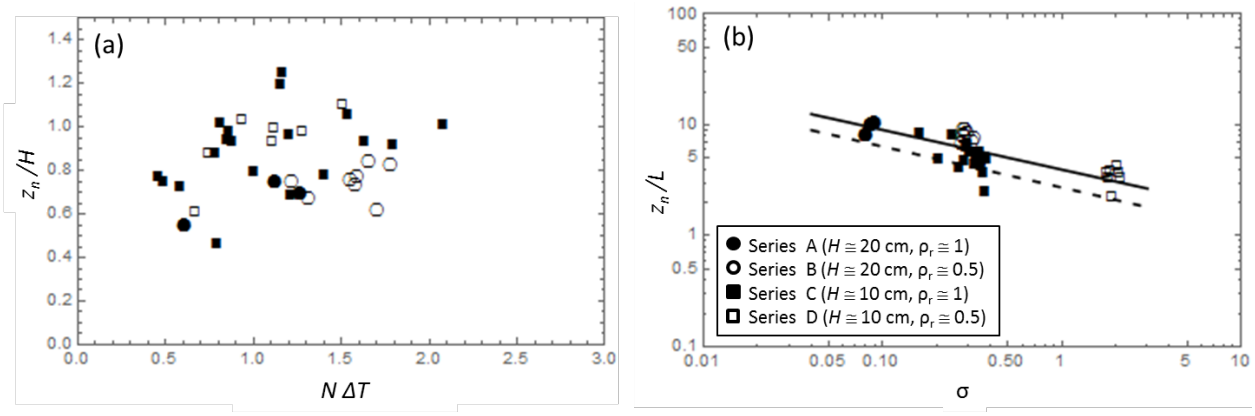

Figure 5. (a) Plume neutral buoyancy depth vs. release duration. (b) Plume neutral buoyancy depth scaled by intrinsic scales.

Fig. 5(a) shows that the final depth, z_n, does not exhibit a clear trend with H or ρ_r,. Scaling z_n with the intrinsic length scale, L_0 and plotting vs. the flux ratio, σ, however, results in a definitive power law trend

$$\frac{z_n}{L_0} = 3.96\,\sigma^{-0.36}\,, \tag{14}$$

shown as a solid line in Fig. 5(b). The evolution of the neutral buoyancy depth with flux ratio is in excellent agreement with the data of Richards *et al.* [15] for a continuous forced plume at $\sigma < 50$

$$\frac{z_n}{L_0} = 2.73\,\sigma^{-0.37}\,, \tag{15}$$

shown as a dashed line in Fig. 5(b). The difference in the pre-factor in (14) and (15) results from the difference in the experimental configurations of the two experiments.

The initial plume energy, computed from (10), is shown in Fig. 6(a). As the momentum of the exiting plume is essentially constant, the increase of E_p with $N\Delta T$ is expected, as are the higher values for the cases with $\rho_r \cong 1$, than those with $\rho_r \cong 0.5$.

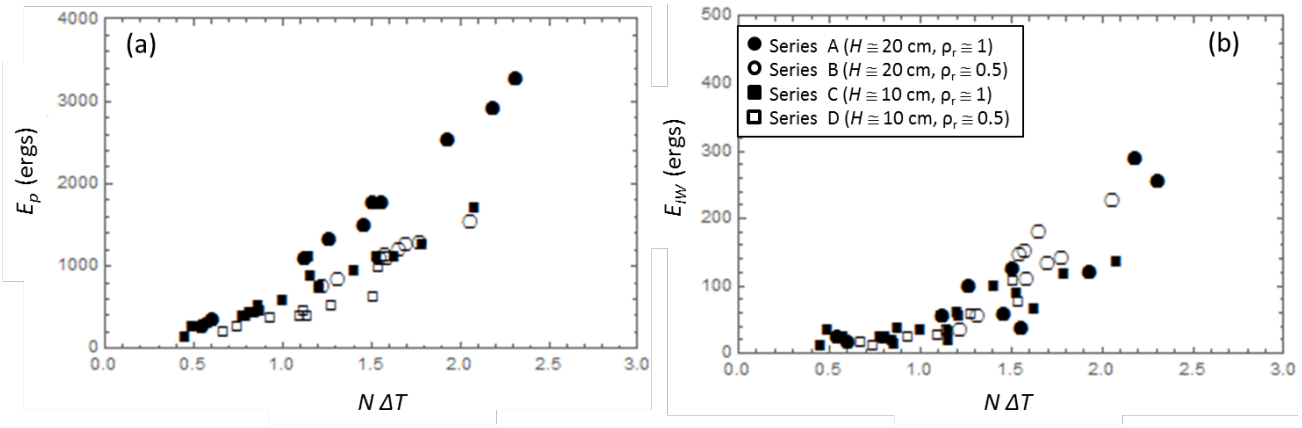

Figure 6. (a) Plume energy vs. release duration. (b) Internal wave energy vs. release duration.

B. Internal wavefield

As the conductivity probe array is positioned at one circumferential location, the measured internal wavefield will vary from run to run due to the variation in specific features of the turbulent plume at that radial location. However, on average, the measured internal wavefield properties within each test series can be considered as representative of the average circumferential pattern and that the variability in the measured internal wavefield energy is the result of the inherent circumferential variations.

Figure 7(a, c) show the internal waves measured at each probe within the stratified layer for two representative runs with the wave displacements increased by a factor of 5 for visual clarity. The red dashed lines show the extent and magnitude of the stratified layer for each case, illustrating the fact that the conductivity probes spanned the entire stratified layer. The bottom charts, Fig. 7(b, d) show the cumulative energy flux, $E_{IW,pe}$, obtained by summation over the probes within the stratified region (note that series with the larger stratified region ($H \cong 20$ cm, Series A and B), have more active probes than the $H \cong 10$ cm series (Series C and D). The black line in Fig. 7(b, d) shows the directly computed energy flux while the overlaid red line shows the data smoothed with a 1 s boxcar filter.

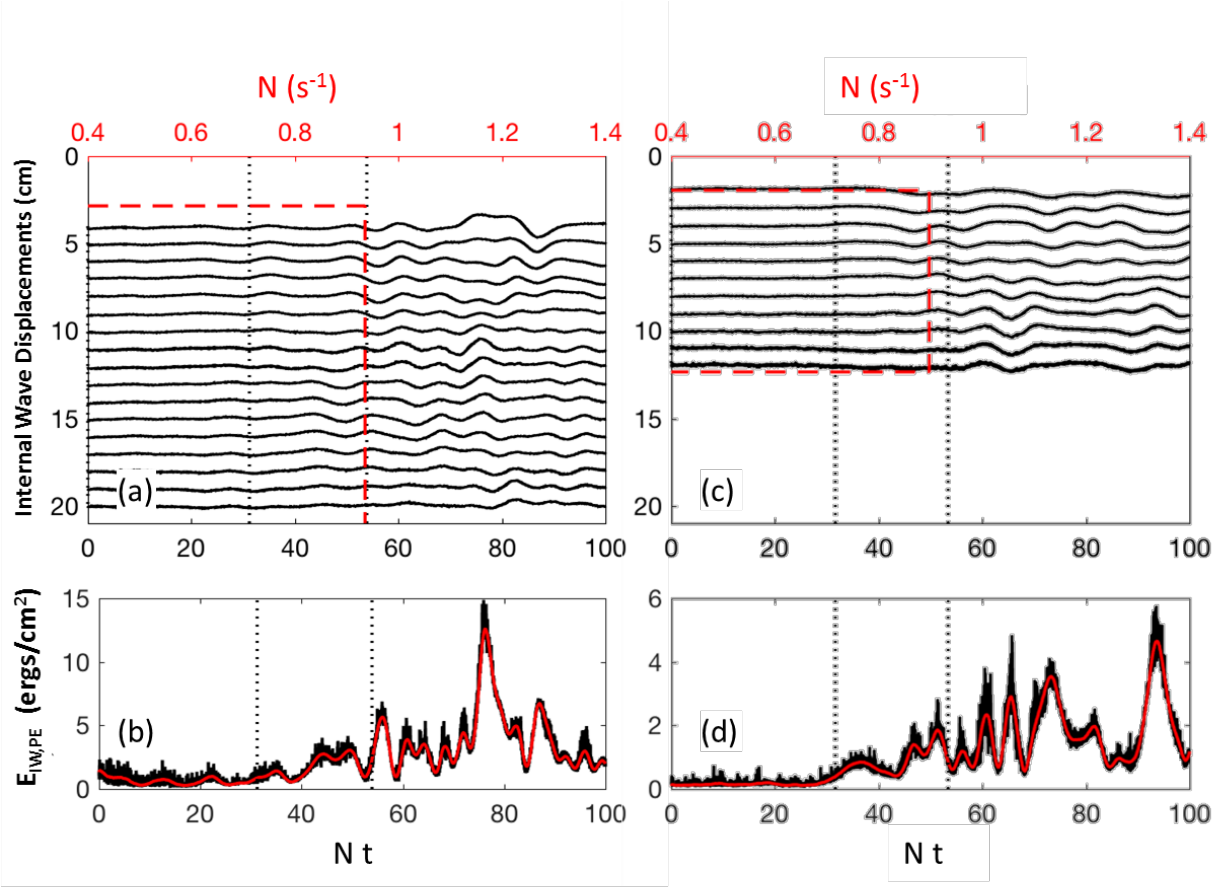

Figure 7. Internal wave displacements and cumulative energy within the stratified layer. (a, b) Series A, Run 3B, H = 21.5 cm, ρ_r = 1.31, ΔT = 1.62 s. (c, d) Series D, Run 84, H = 12.3 cm, ρ_r = 0.44 , ΔT = 1.25 s. Wave displacements in (a, c) are scaled by a factor of 5, for clarity.

The dotted vertical lines in Fig. 7 show the region of valid data. The first line represents the wave onset line, the time at which the energy flux exceeds one standard deviation above the early time background level. Since there is a range of wave speeds within the layer the average over the stratified layer is used to calculate the internal wavefield energy as shown in Fig. 7 (b, d). As the plume generated internal waves were observed to be generated primarily on the plume rebound (as also found in [8, 10]), the internal wave phase speed, c_w, is calculated using the time interval from when the plume reaches the maximum depth, z_{max}, to the time when the waves are first detected (the first dashed line) and the known distance between the plume centerline and the conductivity probe rake. Considering the variability of the internal wavefield due to its turbulent nature the average value for all runs, c_w = 2.31 cm/s, was used.

The second vertical dotted line represents the wave cutoff line, the time at which internal wave reflections from the tank back wall contaminate the measurements, calculated as the time at which internal waves propagating at c_w reflected off the back wall of the tank would reach the probe rake. It is evident in Fig. 7(a, c) that prior to wave onset there is little wave

motion and after the wave cutoff line there is a marked increase in wave activity due to the combined incident and reflected waves. The region of valid data, $\Delta Nt \cong 25$, represents ~4 Brunt-Väisäliä periods (i.e., since $N \cong 1$ s^{-1} so that $T \cong 2\pi$ s) which should be sufficient to capture the initial, most energetic plume generated internal waves, but perhaps not the total internal wavefield energy. Thus, the calculated E_{IW} values should be considered a (slightly) lower bound.

The internal wave amplitudes within the region of valid data are measureable even though quite small, O(1 mm) or less. Over all test runs, the dominant wave period within the valid region is ~10 s to 15 s, yielding $\omega/N \cong 0.4$ to 0.7, values not unlike those found by Ansong and Sutherland [8] where ω/N ranged from 0.45 to 0.85 and Cerasoli [14] where $\omega/N \cong 0.7$.

The energy of the measured internal wavefield, E_{IW}, is computed from (12) and shown in Fig. 6(b). While there is an increase in E_{IW} with $N\Delta T$, as would be expected, there is no discernable effect of changes in H and ρ_r.

C. Energy ratio

The ratio of internal wave energy to the plume initial energy, $\frac{E_{IW}}{E_p}$ is shown in Fig. 8 as a function of Fr_0 ($\propto N\Delta T$). The accuracy of the experimental measurements is indicated by the representative error bar in Fig. 8(a) computed by evaluation of the measurement errors of each of the factors in (10) and (12). The scatter in the data is primarily due to the turbulent nature of the plume as mentioned above.

In contrast to the lack of discernable trends in the evolution of E_{IW} (Fig. 6(b)) the ratio of IW to plume energy, $\frac{E_{IW}}{E_p}$ exhibit significantly different trends dependent on the plume density, i.e. ρ_r . For the heavy plumes, $\rho_r \cong 1$ (Fig. 8(a)), $\frac{E_{IW}}{E_p}$ is essentially independent of Fr_0, while for the $\rho_r \cong 0.5$ series (Fig. 8(b)) $\frac{E_{IW}}{E_p}$ clearly increases with increasing Fr_0. Average values of $\frac{E_{IW}}{E_p}$ for each test series are shown in Table 1. Mean values for all the $\rho_r \cong 1$ and $\rho_r \cong 0.5$ data shown in Fig 8 are 0.065 and 0.101 respectively, with the latter having values as high as 0.15 at high values of Fr_0.

Least-square linear fits to these results are shown as dashed lines, with

$$\frac{E_{IW}}{E_p} = 3.4\ 10^{-5}\ Fr_0 + 0.064 \tag{16}$$

for the $\rho_r \cong 1$ series, showing virtually no dependence on Fr_0, and

$$\frac{E_{IW}}{E_p} = 0.0076\ Fr_0 - 0.011 \tag{17}$$

for the $\rho_r \cong 0.5$ series, showing a significant Fr_0 dependence.

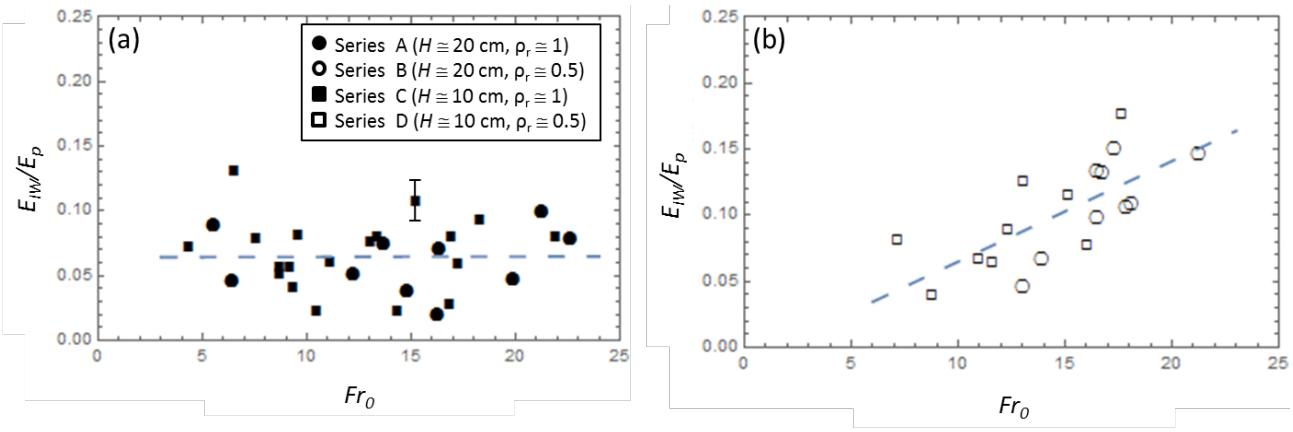

Figure 8. Energy ratio. (a) $\rho_r \cong 1$. (b) $\rho_r \cong$ 0.5.

V. SUMMARY AND DISCUSSION

A series of laboratory experiments with a focus on short duration impulsive, forced plumes and the generation of internal waves within a finite thickness stratified layer were performed. This is the first study where the extent of energy transfer to the internal wavefield by an impulsive plume has been measured. It was found that the general nature of the coupling of the plume energy to the internal wavefield depended primarily on the density of the plume in relation to the ambient stratification. The degree of coupling was found to be of order 8% - 10% in line with other investigations of internal wave forcing from continuous sources.

Internal waves were found to be generated primarily when the descending plume rebounds from its maximum depth and oscillates about a shallower neutral depth, as illustrated in Fig. 7. While there was considerable variability in the extent of plume energy transferred to internal waves, it was found to be independent of the thickness of the stratified layer and instead dependent on the plume density at its release. Plumes with a density that matched that of the bottom of the stratified layer had a constant fraction of the plume energy transferred to the internal wavefield, with an average value of $\frac{E_{IW}}{E_p} \cong$ 6%, independent of the duration of the plume release, while in contrast, plumes with lower densities, half that of the bottom of the stratified layer, exhibited larger plume energy coupling to the IW field that increases with the duration of the plume release and had an average value of $\cong$ 10%.

The present results can be compared to the degree of coupling from turbulent sources into internal waves found in other investigations. The present levels of energy transfer to the IW field lie between the large values (20% -25%) found by Cerasoli [14] and the lower values found for continuous plumes, jets and turbulence forcing [8, 11, 18]. For a turbulent wake of a towed body in a linearly stratified fluid (as opposed to lee wave IW forcing at low *Fr*), it was found that the fraction of the input energy imparted to the potential energy of the internal wavefield was $\propto Fr^{-2}$ with a maximum of ~10% at $Fr \cong 1$ (Brandt and Rottier [16]). Clearly the degree of

turbulent energy that is transferred into internal waves is significant and is highly dependent on the nature of the turbulent source.

In contrast to prior studies, the current experiments considered turbulent-IW coupling resulting from an impulsive source. In all cases the forcing was turbulent and incoherent. Further studies, currently in progress, are considering a coherent impulsive turbulent forcing source, i.e. the propagation of a turbulent vortex ring through a stratified layer, in order to contrast the extent of internal wave generation to that of the incoherent turbulent plume considered herein.

ACKNOWLEDGMENTS

The support of Gary Frederick in configuring and conducting the experiments is greatly appreciated. Curtis Saunders effort to review and improve the manuscript is appreciated. We also appreciate the support of the Office of Naval Research Turbulence and Stratified Wakes program.

---

[1] J. S. Turner, Buoyant plumes and thermals, Ann. Rev. Fluid Mech. **1***,* 29-44 (1969).

[2] A. W. Woods, Turbulent plumes in nature, Ann. Rev. Fluid Mech. **42**, 391-412 (2010).

[3] E. J. List, Turbulent jets and plumes, Ann. Rev. Fluid Mech. **14**, 189-212 (1982).

[4] N. B. Kaye, Turbulent plumes in stratified environments: A review of recent work, Atmosphere-Ocean **46**, 433-441 (2008). doi:10.3137/AO923.2008

[5] G. R. Hunt and H. C. Burridge, Fountains in industry and nature, Ann. Rev. Fluid Mech. **47**, 195-220 (2015).

[6] B. R. Morton, G. Taylor and J. S. Turner, Turbulent gravitational convection from maintained and instantaneous sources, Proc. Roy. Soc. London, A **234**, 1-23 (1956).

[7] B. R. Morton, Forced plumes, J. Fluid Mech. **5**, 151-163 (1959).

[8] J. K. Ansong and B. R. Sutherland, Internal gravity waves generated by convective plumes, J. Fluid Mech. **648**, 405-434 (2010).

[9] R. B. Stull, internal gravity waves generated by penetrative convection, J. Atm. Sci. **33**, 1279-1286 (1976).

[10] T. I. McLaren, A. D. Pierce, T. Fohl and B. L. Murphy, An investigation of internal gravity waves generated by a buoyantly rising fluid in a stratified medium. J. Fluid Mech. **57***,* 229-240 (1973).

[11] E. Ezhova, C. Cenedese and L. Brandt, Interaction between a vertical turbulent jet and a thermocline, J. Phys. Oceanog. **46**, 3415-3437 (2016). doi: 10.1175/JPO-D-16-0035.1

[12] T. L. Clark, T. Hauf and J. P. Kuettner, Convectively forced internal gravity waves: Results from two-dimensional numerical experiments, Q. J. Royal Met. Soc. **12**, 474, 899-925 (1986).

[13] Y. Noh, H. J. S. Fernando and C. Y. Ching, Flows Induced by the impingement of a two-dimensional thermal on a density interface, J. Phys. Oceanog. **22**, 1207-1220 (1992).

[14] C. Cerasoli, Experiments on buoyant-parcel motion and the generation of internal gravity waves, J. Fluid Mech. **86**, 247-271 (1978).

[15] T. S. Richards, Q. Aubourg and B. R. Sutherland, Radial intrusions from turbulent plumes in uniform stratification, Phys. Fluids **26**, 17 pp. (2014). doi: 10.1063/1.4869119

[16] A. Brandt and J. R. Rottier, The internal wavefield generated by a towed sphere at low Froude number, J. Fluid Mech. **796**, 103-129 (2015). doi:10.1017/jfm.2015.96

[17] H. E. Gilreath and A. Brandt, Experiments on the generation of internal waves in a stratified fluid, AIAA J. **23**, 693-700 (1985).

[18] J. R. Munroe and B. R. Sutherland, Internal wave energy radiated from a turbulent mixed layer, Phys. Fluids **26**, 096604 (2014); doi: 10.1063/1.4895645